TECHNICAL NOTE

COMPUTATIONAL INVESTIGATION OF SUPERSONIC JET SCREECH IN CIRCULAR JETS USING HIGHER-ORDER WENO SCHEME

M. Dharani* and A. Chatterjee**

Abstract

Computational investigation of supersonic jet screech in imperfectly expanded circular jets is conducted using higher order Weighted Essentially Non-Oscillatory (WENO) scheme based solution of the axisymmetric Navier Stokes equations. The jet screech phenomenon is numerically simulated for an over expanded and an under expanded circular supersonic jet. Sound pressure levels, screech amplitude and frequency are calculated from the pressure history in the flow field and compared with values in literature. Shock cell spacings in the high speed jet are also extracted from numerical simulations and compared with that in literature. Important aspects of a screeching jet observed experimentally, like the interaction of instability waves with the shock train and the contribution of downstream propagating hydrodynamic fluctuations to the creation of the upstream moving acoustic wave in the acoustic feedback mechanism, are also captured in the present computations. The latter phenomenon has been observed experimentally but not reported previously in numerical simulations.

Nomenclature

c = speed of sound
C_p = specific heat at constant pressure
D = nozzle diameter
e = internal energy
f = numerical flux function
F,G = flux vectors
i = grid point
k = ENO stencil
L = shock spacing
M = Mach number
p = pressure
Pr = Prandtl number
q = heat flux vector
Q = source term vector
Re = Reynolds number
S = strain rate tensor
t = time
T = temperature
u = stream wise component of velocity
U = vector of conservative variables
v = radial component of velocity
w = weights
x = stream wise coordinate
y = radial coordinate
γ = ratio of specific heats
μ, μ_t = viscosity, eddy viscosity
ρ = density
τ = stress tensor

Subscripts

e = nozzle exit value
i = inviscid
j = perfectly expanded nozzle exit value
v = viscous
∞ = freestream

Introduction

Screech noise emitted from a high-speed jet was first studied at length by Powell [1, 2, 3]. The theory proposed by Powell almost fifty years ago is still widely accepted as the formal explanation on the generation of screech in high-speed jets. The noise production in imperfectly expanded supersonic jets is partly due to the interaction between jet instability waves and the shock-cell structure. If no counter-measures are taken, the emitted shock associated noise can re-excite certain instability wave modes at the nozzle lip and cause resonance feedback to occur. This feedback resonance, known as supersonic jet screech,

* Graduate Student, Presently working in Fluent India
** Associate Professor, Department of Aerospace Engineering Indian Institute of Technology Bombay, Powai Mumbai-400 076, India; Email : avijit@aero.iitb.ac.in
Manuscript received on 28 Sep 2004; Paper reviewed, revised and accepted on 07 Oct 2005

cause the jet to flap violently at discrete frequencies and generates very strong, narrow band tones (screech tones). Jet screech was shown to be a source of acoustic fatigue failure in the tail and nozzle structures of supersonic aircraft. Such fatigue failure have been observed in high performance aircraft like VC-10, F-15 and B1-B [4]. Jet screech has been the focus of extensive experimental investigations which has led to important details of the jet screech mechanism. Experiments reveal that the mechanism for sound production is fundamentally different and more efficient when the instability waves are the large organized eddies that are typical of screech then when they are small disturbances. Analytical models have been proposed which can predict screech frequency to satisfactory level but screech amplitude still requires to be experimentally or numerically evaluated.

High-resolution, non-oscillatory shock capturing schemes are an attractive option for investigating the jet screech phenomenon. Essentially Non-Oscillatory (ENO) [5] and Weighted Essentially Non-Oscillatory (WENO) [6] techniques are well known for successfully resolving flow fields containing shock waves, acoustic waves and complicated smooth flow structures typical of the jet screech phenomenon. In the current work, a fifth order accurate WENO based technique is used to solve the axisymmetric Navier-Stokes equations to numerically simulate axisymmetric screech modes issued from imperfectly expanded circular supersonic jets. Initially computations are carried out for a perfectly expanded Mach 2 jet for which experimental results were presented by Seiner et al [7] and subsequently investigated numerically by Rona et al. [8]. This is followed by computations involving imperfectly expanded jets. The formation of shock cells in the high-speed jet enclosed by the shear layer and convecting instability waves which are basic ingredients of a screeching jet are captured in computations for an over expanded jet with M_e (the jet exit Mach number) = 2 and M_j (the corresponding perfectly expanded jet exit mach number) = 1.49. The shock cell spacing in the jet is compared with experimental and numerical values reported in literature. The screech frequency computed is compared with that obtained from Powell's formula [3] and the screech amplitude is compared with values also predicted numerically by Rona et al. [8]. Computations are then carried out for a under expanded jet with M_e = 1 and M_j = 1.19. Quantitative data regarding screech amplitude and frequency obtained from spectral analysis are compared with values predicted numerically by Jorgensen et al. [9] and that measured by Ponton et al. [10] for this problem. Computations also capture the creation of acoustic fluctuations due to the interaction of downstream moving hydrodynamic fluctuations in the shear layer with upstream moving acoustic waves. These acoustic waves are a part of the resonance feedback mechanism in screeching jets. This interaction between the downstream moving hydrodynamic fluctuation and the upstream moving acoustic waves has been studied experimentally by Panda [11] for similar conditions but such observations have not been previously reported in numerical simulations.

Governing Equations and Numerical Scheme

Axisymmetric Navier-Stokes equations with a simplified large eddy simulation (LES) model similar to that used by Jorgenson et al. [9] is used to numerically simulate perfectly expanded, over expanded and under expanded jets emitted by a circular nozzle. The perfectly expanded jet is computed for $M_e = 2$, and is symmetric about the central axis as noted by Seiner et al. [7]. The screech modes associated with the under expanded jet with $M_j \leq 1.19$ simulated here is also axisymmetric in nature [12]. In case of the over expanded jet with $M_j = 1.49$, also solved here, Seiner et al. [13] observed both axisymmetric and helical shear layer instabilities which is not captured in an axisymmetrical model. However, given the fundamentally similar nature of the self-sustained instability mechanism for both axisymmetric and non-axisymmetric modes, it is still possible to get and insight into the screech phenomenon for the over expanded jet by simulating the axisymmetric modes [8].

The governing equations for the time-dependent axisymmetric Navier Stokes equations are written as

$$\mathbf{U}_t + \mathbf{F}_x + \mathbf{G}_y = \mathbf{Q}, \tag{1}$$

x and y are the streamwise and radial coordinates respectively and t denotes time. **U** is the vector of conservative variables, **F** and **G** the flux vectors in the streamwise and radial directions respectively and **Q** the source term due to axisymmetry. The variables in the state vector in equation (1) are :

$$U_1 = \rho,\ U_2 = \rho u,\ U_3 = \rho v,$$
$$U_4 = p/(\gamma - 1) + \rho(u^2 + v^2)/2,$$

where ρ, u, v, p, and γ are the density, streamwise component of velocity, radial component of velocity, static pressure, and constant specific heat ratio, respectively. The flux vectors split into inviscid and viscous fluxes are :

$\mathbf{F = F_i - F_v}$, $\mathbf{G = G_i - G_v}$

Inviscid and viscous fluxes are given by :

$$\boldsymbol{F_i} = \begin{bmatrix} \rho u \\ \rho u^2 + p \\ \rho uv \\ (\rho e + p)\, u \end{bmatrix}, \quad \boldsymbol{G_i} = \begin{bmatrix} \rho v \\ \rho uv \\ \rho v^2 + p \\ (\rho e + p)\, v \end{bmatrix},$$

$$\boldsymbol{F_v} = \begin{bmatrix} 0 \\ \sigma_{xx} \\ \tau_{xy} \\ u\sigma_{xx} + v\tau_{xy} + q_x \end{bmatrix} \text{ and } \boldsymbol{G_v} = \begin{bmatrix} 0 \\ \tau_{xy} \\ \sigma_{yy} \\ u\tau_{xy} + v\sigma_{yy} + q_y \end{bmatrix} \quad (2)$$

Various terms in viscous fluxes are given by :

$$\sigma_{xx} = -\frac{2}{3}(\mu \nabla . U) + 2(\mu \frac{\partial u}{\partial x}),$$

$$\sigma_{yy} = -\frac{2}{3}(\mu \nabla . U) + 2(\mu \frac{\partial v}{\partial y}),$$

$$\tau_{xy} = \mu\left(\frac{\partial v}{\partial x} + \frac{\partial u}{\partial y}\right),$$

$$\nabla . U = \frac{\partial u}{\partial x} + \frac{\partial v}{\partial y} + \frac{v}{y},$$

$$q_x = -C_p\left(\frac{\mu}{Pr}\right)\left(\frac{\partial T}{\partial x}\right), \; q_y = -C_p\left(\frac{\mu}{Pr}\right)\left(\frac{\partial T}{\partial y}\right)$$

where C_p, T, Pr and μ are the specific heat at constant pressure, temperature, Prandtl number, and viscosity, respectively. The source term is given as :

$$Q_1 = -G_1/y, \; Q_2 = -G_2/y,$$

$$Q_3 = p + \frac{2}{3}\mu(\nabla . U) - 2\mu\left(\frac{v}{y}\right) - G_3/y,$$

$$Q_4 = -G_4/y$$

A simplified LES model [9, 15] is incorporated in the current numerical formulation to handle the strong momentum exchange which takes place in the shear layer. In this simplified model, the system of equations (1) are considered to be the filtered equations governing the resolved scales recovered through a Favre averaging process. The additional unresolved or subgrid terms are modeled as source terms to these equations. A simple Smagorinsky subgrid scale model is used to define the eddy viscosity μ_t and is given by

$$\mu_t = (C_s \Delta)^2 (2S_{ij} S_{ij})^{1/2} \quad (3)$$

where

$$S_{ij} = \frac{1}{2}\left(\frac{\partial u_i}{\partial x_j} + \frac{\partial u_j}{\partial x_i}\right),$$

with $\Delta = (\Delta x\, \Delta y)^{1/2}$ and $C_s = 0.1.\mu + \mu_t$ replaces μ in the computations. The Smagorinsky model is an eddy viscosity model where the subgrid scale stress tensor is modeled as an eddy viscosity multiplying the resolved stress tensor. Replacing μ by $\mu + \mu_t$ results in the addition of the source terms which models the effect of the unresolved or subgrid terms to the filtered momentum equations. The momentum equation in the streamwise and radial directions in the current simplified LES formulation ignores the compressibility correction term [14] that would have been present in a more complete LES modeling for compressible flow. Similarly the subgrid turbulent dissipation rate in the energy equation has not been modeled in the present simplified LES formulation. It is also assumed that the subgrid scale Prandtl number equals the laminar Prandtl number P_r (= 0.72). This simplified LES model has earlier been successfully used in the near-field screech tone analysis of supersonic axisymmetric jets [9,15].

WENO Scheme

WENO schemes [6] are an extension of the successful ENO technique for obtaining higher-order accurate and non-oscillatory resolution for flowfields with discontinuities. The ENO scheme belongs to the class of high resolution numerical schemes developed to deal with flow fields containing shock waves, and are able to maintain high order accuracy in smooth regions of the flow as well as provide for non-oscillatory shocks. The ENO scheme is able to achieve this dual capacity by employing an adaptive stenciling procedure. The adaptive stenciling attempts to make use of the smoothest possible information in the computation of the numerical fluxes at the cell interfaces. The points in the stencil that contribute to the computation of numerical fluxes at cell interfaces for the next time step are chosen in a nonlinear manner and depend on the instantaneous solution. In the ENO stencil choosing process, k candidate stencils are considered covering ($2k$ - 1) cells but only one of the stencil is actually used in defining the numerical flux function. If all the $2k$ - 1 cells in the potential stencil are used, then $(2k\text{-}1)^{th}$ order accuracy in

smooth regions can be obtained. Hence, instead of using only one of the candidate stencils to form the reconstruction, WENO schemes use a convex combination of all the WENO candidate stencils to form the numerical flux function (at cell interface i+1/2) as

$$\hat{f}_{i+\frac{1}{2}} = \sum_{r=0}^{k-1} w_r \, f^{(r)}_{i+\frac{1}{2}}, \quad (r = 0, 1, ..., k-1). \tag{4}$$

Each of the candidate stencils is assigned a weight w_r which determines the contribution of the stencial to the final approximation of the numerical flux. The weights are defined such that in smooth regions it approaches optimal weights to achieve a higher-order of accuracy (a k^{th} order ENO scheme leads to a $(2k\text{-}1)^{th}$ order WENO scheme in smooth regions). Near discontinuities the stencils are assigned a nearly zero weight. Thus, essentially non-oscillatory property is achieved by emulating ENO schemes around discontinuities and a higher-order of accuracy is obtained by emulating upwind central schemes with optimal weights away from the discontinuities [6]. A spatially fifth order accurate WENO technique is used in the current work along with second order Runge Kutta time stepping.

Perfectly Expanded Jet

The nozzle geometry and computational domain for the perfectly expanded jet and the over expanded jet is the same and is shown in Fig.1. Inviscid solid wall boundary conditions are implemented at the axis of symmetry and non-reflecting boundary conditions (NRBC) at outflow boundaries similar to that in Ref. [9]. Ambient conditions in the flow domain are 101320 N/m^2, 288.15 K, and 0 m/s for pressure, temperature, and velocity respectively. A perfectly expanded jet at $M_e = 2$ is obtained when the nozzle exit conditions are set to p_e = 101320 N/m^2, T_e = 162.81 K, ρ_e = 2.168 kg/m^3 and u_e = 511.5 m/s. The Reynolds number (Re) based on the jet diameter is 5x10^6. This problem has previously been numerically investigated by Rona et al. [8] with axisymmetric Navier Stokes solution based on the κ-ω turbulence model and is also similar to that studied experimentally by Seiner et al. [7].

The time dependent numerical simulation is started from stagnant ambient flow conditions. Computations were advanced by a fixed time step to a normalized time of 140 (time normalized by D/u_e with D the nozzle diameter), and this total time was enough to exit the initial flow at the nozzle through the right hand boundary of the computational domain. The flow variables were time averaged between normalized times of 140 to 290, and this time period was sufficient to damp the unsteady fluctuations in the flow field. Initially computations were performed on two uniform discretizations corresponding to 420 x 140 cells and 420 x 280 cells. Fig.2 compares results obtained for axial flow velocity (normalized by u_e) at the jet axis with experimental values [7]. The discretization 420 x 280 predicts the axial flow velocity variation closer to experimental results compared to that on a 420 x 140 grid, and all further computations are carried out on an uniform discretization consisting of 420 x 280 cells.

Theoretically, a perfectly expanded inviscid jet is free from shocks as indicated in the time-averaged inviscid Euler prediction in Fig.2. When Navier-Stokes computations are carried out, the flow field near the nozzle lip contain weak shock cells due to which there are velocity fluctuations at the nozzle exit. Similar fluctuations in the normalized velocity are seen in the experiment carried out by Seiner et al. [7] (Fig.2) and also in axisymmetric Navier stokes computations of Rona et al. [8]. The formation of shock cells in experiments can be attributed to fluctuation in the reservoir pressure and boundary layer formation near the nozzle lip.

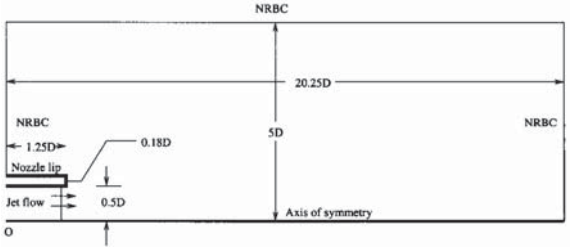

Fig. 1 Computational domain, perfectly and overexpanded jet

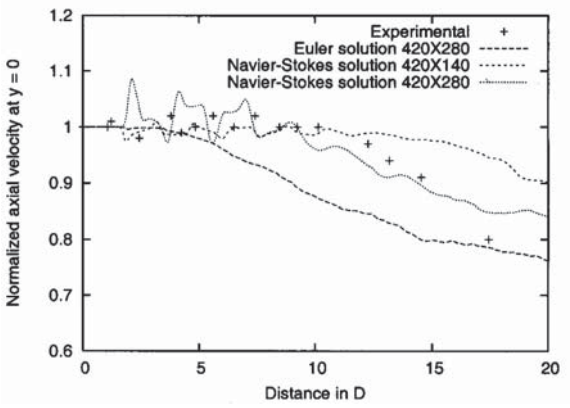

Fig. 2 Time averaged axial velocity profile (y=0), perfectly expanded jet

The time mean experimental results show that the high speed core of the jet terminates around D ~ 10 and the axial velocity starts decaying thereafter. The time averaged computational result shows good match upto D ≤ 8. The decay rate of axial velocity is slower in the computational predictions as compared to experimental results (Fig.2). The shear layer spread can be quantified by the half velocity point $y_{0.5}$, where $y_{0.5}$ is the radial distance at which axial velocity is half the jet axis velocity. The computational predictions show a similar trend to that of experimental results [16] as shown in Fig.3.

Over Expanded Jet

The nozzle geometry, computational domain, ambient flow conditions for the over expanded jet are same as in case of perfectly expanded jet. An over expanded jet is obtained by reducing the nozzle pressure ratio from $p_e/p_\infty = 1$ to $p_e/p_\infty = 0.46$. The nozzle exit conditions are set to T_e = 162.78 K, p_e = 46632 N/m^2, u_e = 511.5 m/s, M_e = 2 and Re = 2.3 x 10^6 which is identical to that investigated numerically in Ref. [8] using κ-ω turbulence model based axisymmetric Navier Stokes solution.

Due to the pressure difference between the nozzle exit and the ambient, the high speed core of the jet near the nozzle lip has shock cells as seen in the time averaged density, and axial velocity contours in Fig.4. The shear layer from the nozzle lip causes multiple reflections resulting in a sequence of shock and expansion waves in the jet bounded by the shear layer with decreasing shock strength in the streamwise direction. Downstream at $x \geq 6D$, the flow is free from shock and expansion waves. The velocity contour also shows the shear layer growth in the over expanded jet. The over expanded jet shear layer is comparatively thin upto $x \leq 4D$ and starts growing after that as can be seen in Fig.4. Similar observations have been made in the numerical investigation in Ref. [8].

The shock cell sequence for an over expanded jet should start with a shock at the nozzle lip as can be seen in the time averaged normalized pressure measurements in Figs. 5 and 6 which show four shocks of significant strength. The figures show that the strength of the first shock is maximum after which there is a monotonic decrease in the shock strength. The amplitude and location of first shock is predicted well by the numerical technique while the location of the second, third, and fourth shock is predicted better compared to the amplitude. The amplitude of these shocks are under-predicted as compared to experimental values [17] in both locations as seen in Figs.5 and

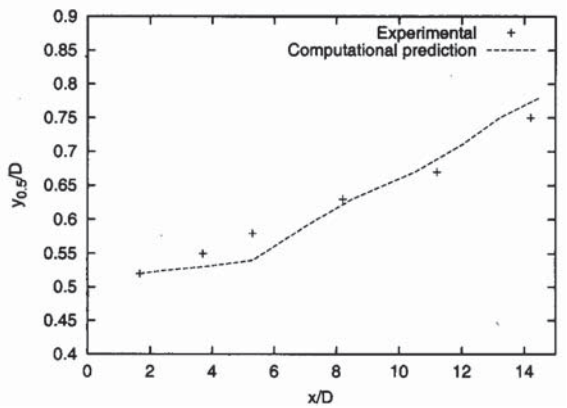

Fig. 3 Half velocity points, perfectly expanded jet

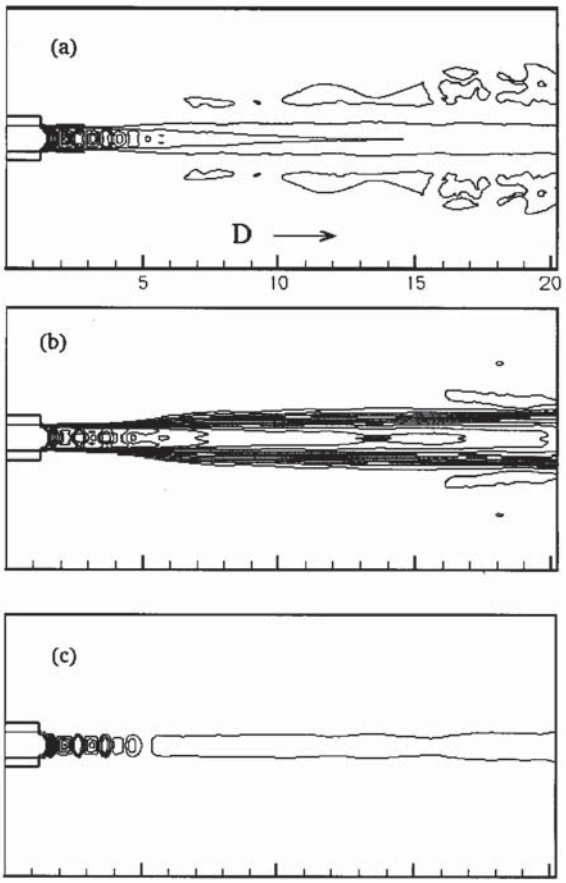

Fig. 4 Time averaged contour plots, (a) density (b) axial velocity (c) pressure, overexpanded jet

Table-1 : Comparison of shock cell spacing, overexpanded jet

Shock Spacing	Present Prediction	Prediction by Rona et al. [8]	Measurement by Norum et al. [17]	Empirical Value by Seiner et al. [18]
L_1/D	1.00	1.00	1.00	-
L_2/D	0.97	1.00	0.94	1.09
L_3/D	0.93	0.95	0.83	-
L_{ave}/D	0.95	0.97	0.9	0.88

Table-2 : Comparison of screech amplitude (in db) and frequency (in Hz), underexpanded jet

Screech Quantity	Present Prediction	Numerical Prediction [9]	Measurement by Ponton et al. [10]
Amplitude	139	130	136
Frequency	8500	8600	8200

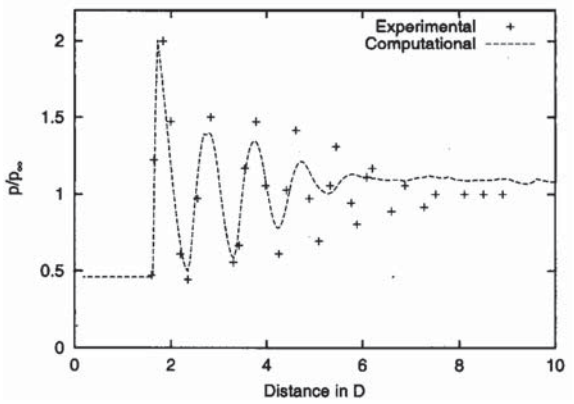

Fig. 5 Time averaged normalized pressure (jet axis), overexpanded jet

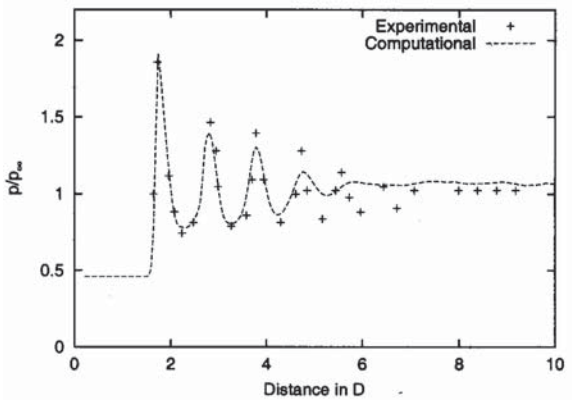

Fig. 6 Time averaged normalized pressure (y=0.25D), overexpanded jet

6. Along the axis, sharp pressure maxima and sharp pressure minima are observed while along y = 0.25D line, sharp pressure peaks and rounded pressure minima are observed consistent with computational results of Rona et al. [8]. Table-1 shows comparison of shock cell spacing between present prediction, numerical predictions of Rona et al. [8], time averaged experimental measurement by Norum et al. [17], and expirical relationship by Seiner et al. [18]. Computational predictions and experimental measurements show a decreased shock spacing as the location of shock cell moves away from nozzle lip. The shock cell length reduces due to the shear layer convexity and decreasing axial mean flow speed which reduces the shock angle within successive cells [17]. Good agreement is found between the measured and predicted spacing (L) up to the third cell (L_3) in the present computations.

The pressure contour plots in Fig.7 show the shear layer containing series of shock cells and large scale instability waves. Arrow "I" shows the formation, propagation and amplification of instability waves in the shear layer. The shocks in the flow field are indicated by integers with arrow heads. It can be seen that the location of first shock is almost fixed and the instability wave "I" does not show its presence near the first shock. The instability wave starts developing as it passes the second shock and becomes fully developed on reaching the third shock (Figs. 7b to 7d). The amplified instability wave interacts with shock as shown in Figs.7c and 7f. These interaction causes the shock to move over its mean position and such shock movement is significant in the third and fourth shock where the instability waves are amplified. The shock movement causes the shock to smear in the time averaged measurement [8] as in Fig.5 with the amount of smearing

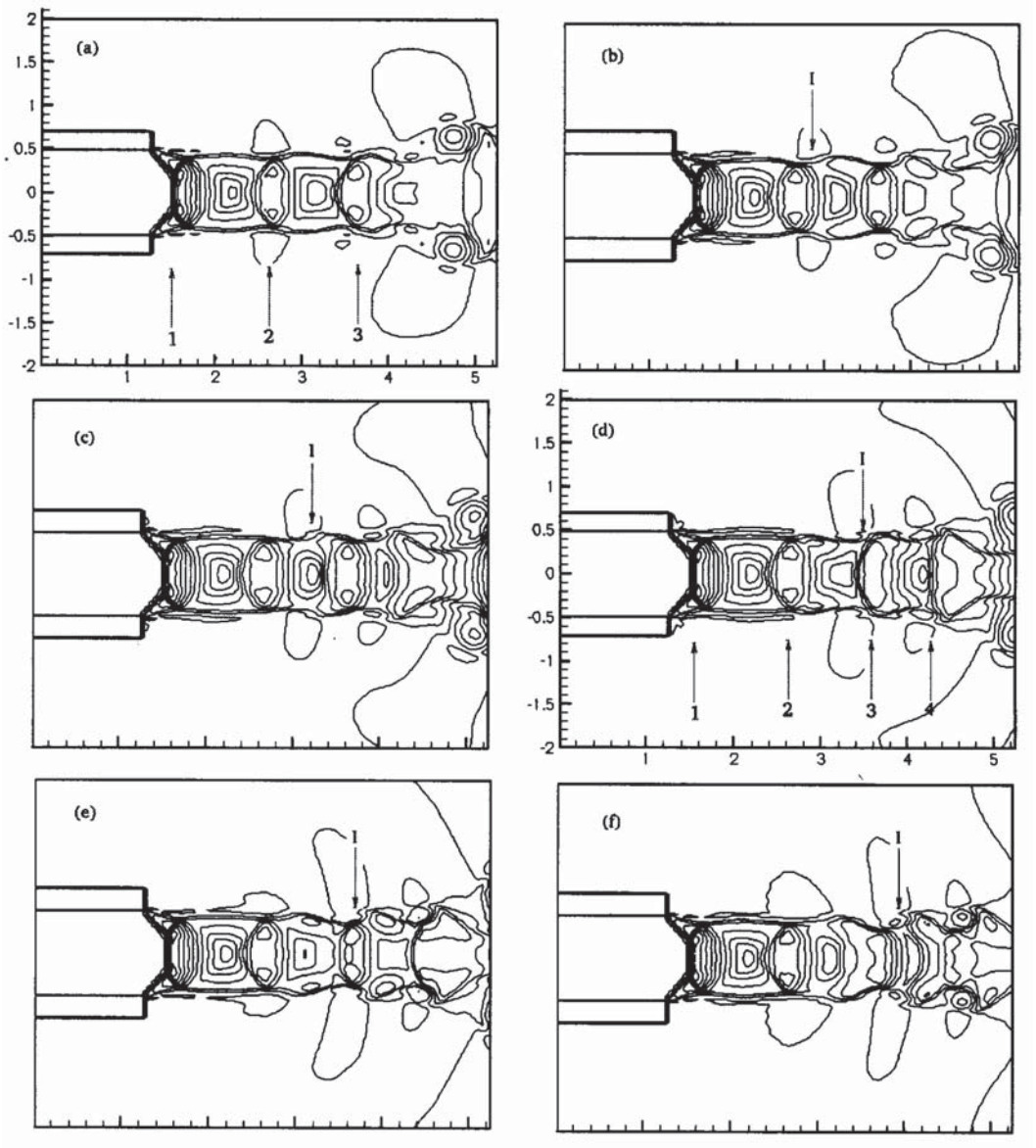

Fig. 7 Pressure counters at equal time interval of 5×10^{-5} sec, overexpanded jet

depending on the amplitude of shock oscillation. Shock oscillation and its contribution to screech generation has been extensively analysed by Panda [12] for under expanded jets. It should be noted that these unsteady computations like the axisymmetric computations of Rona et al. [8] capture only the toroidal instabilities. The helical instabilities in the experiments of Seiner et al. [13] are not captured in an axisymmetric model.

The time dependent pressure fluctuations in the present computations as well as in Ref.[8] are measured at two locations, one being on the jet axis at x = 5D, and other at x = 5D and y = 0.25D and the overall pressure levels measured correspond to 178.5 db and 180.0 db (with reference level of 20 μPa) respectively. These values are 5 dB higher than axisymmetric Navier Stokes based predictions of Rona et al. [8] with $k - \omega$ turbulence model at the same location. The unsteady pressure fluctuation at

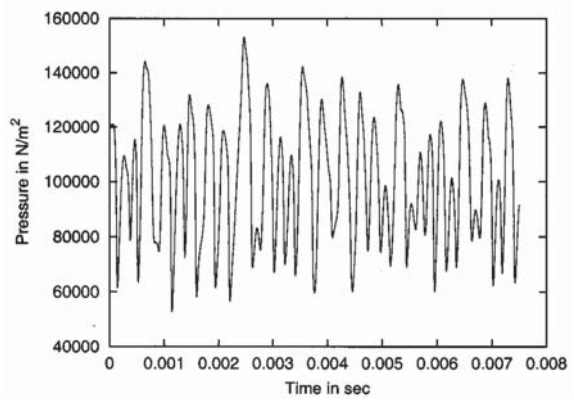

Fig. 8 Pressure fluctuations (x=5D, y=0.25D), overexpanded jet

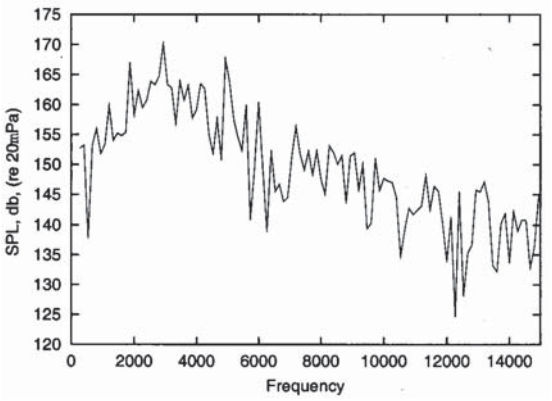

Fig. 9 Sound pressure level (x=5D, y=0.25D), overexpanded jet

(5D, 0.25D) is shown in Fig.8 and analyzed spectrally using a discrete Fourier transform (DFT). The resulting sound pressure level (SPL) is shown in Fig.9. There are multiple spikes in the spectrum and the spike at 3000 Hz has the maximum amplitude of 171 db. This frequency and amplitude correspond to screech. The dominant screech frequency predicted by Powell's formula [3] for this case is 3500 Hz and is 500 Hz higher than present predictions.

Under Expanded Jet

The nozzle geometry and computational domain are shown in Fig.10, and an uniform discretization corresponding to 700 x 300 is used. The initial conditions in the computational domain other than nozzle exit are taken to be stagnant atmospheric conditions, with atmospheric pressure p_∞ = 101320 N/m^2, temperature T_∞ = 288 K and density ρ_∞ = 1.225 Kg/m^3. The outflow jet conditions are such than M_e = 1, and M_j = 1.19. At the nozzle exit, the jet expands into the atmosphere at sonic speed with elevated density and pressure. The pressure, density and axial velocity are 128119.35 N/m^2, 1.8591 kg/m^3, and 310.61 m/sec, respectively. Time is normalized by D/c_∞ (c_∞ the ambient speed of sound), the initial flow was allowed to leave the computational domain and time averaging was carried out between normalized time 24 to 54. This problem has also been simulated numerically by Jorgenson et al. [9]. Experimental results for an axisymmetric under expanded supersonic jet at M_j = 1.19 for which the screech mode is axisymmetric has been presented by Panda [12] and Ponton et al. [10].

The high speed jet flow coming out of the nozzle is under expanded with nozzle outlet pressure higher than the atmospheric pressure which results in a sequence of

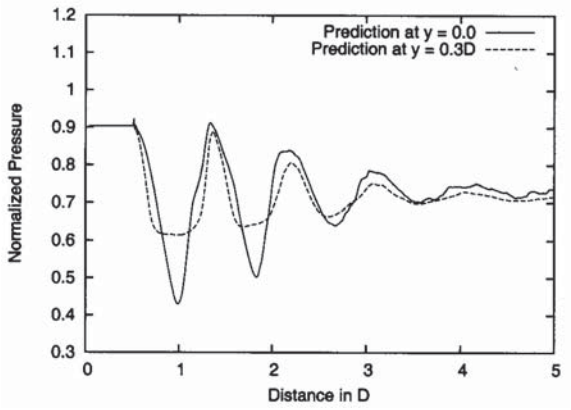

Fig. 11 Time averaged pressure (y=0 and y=0.3D), underexpanded jet

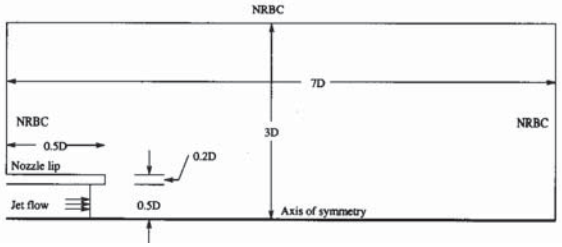

Fig. 10 Computational domain, underexpanded jet

expansion waves and shock waves in the jet as shown in the time averaged pressure plot in Fig.11. For an under expanded jet the initial wave at the nozzle exit is an expansion wave and as in an over expanded jet the shock strength decreases with increasing distance from the nozzle lip and can be seen in Fig.11. The first shock wave is relatively sharper compared to the rest and this could be

due to lack of instability in the shear layer close to first shock. The instability waves starts growing after the first shock and becomes amplified as it moves downstream. These amplified instability waves cause shock waves in the shock train to oscillate [12] which smears the shock in the time averaged results. The average shock spacing in the present computation is 0.85D and is 10% higher than the experimental value obtained by Panda [11].

A discrete Fourier transform is carried out on the unsteady pressure data to obtain screech frequency and amplitude. The unsteady pressure history is recorded at the nozzle lip, at a radial distance of 0.642D from the jet axis. Experimental and numerical results at the same location for the geometry being modeled is available in Ref. [10] and Ref. [9] respectively. Fig.12 shows the sound pressure level obtained from the spectral analysis. Table-2 compares the predicted screech amplitude and frequency for the dominant mode (also known as the A2 mode in literature) from the present computations with that in Refs. [10] and [9]. It may be noted that Fig. 12 also contains strong subharmonics to the left similar to that in numerical predictions for this geometry in Ref.[9] using an axisymmetric formulation. It is observed that results from present computations slightly over predict both screech frequency and amplitude as compared to experimental results in Ref. [10].

In the screech noise mechanism the acoustic waves move primarily in the upstream direction while the organized structures in the shear layer move in the opposite downstream direction. The downstream moving hydrodynamic fluctuations in the shear layer and upstream propagating acoustic waves are shown in series of contour plots in Fig.13. The rarefied regions are shown in dashed con-

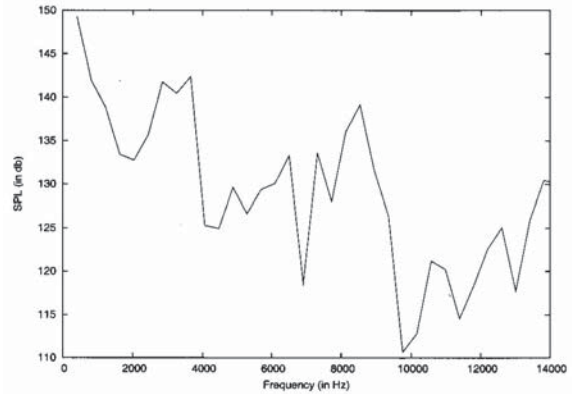

Fig. 12 Sound pressure level (x=0.5D, y=0.642D), underexpanded jet

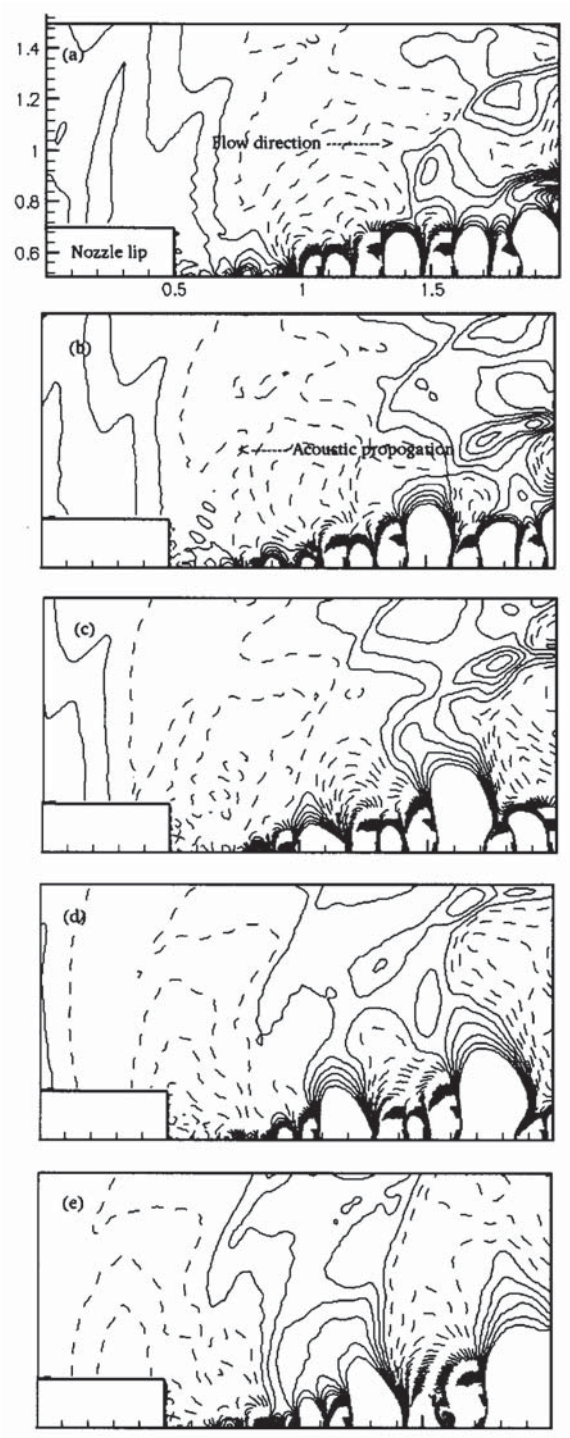

Fig. 13 Pressure contours at equal normalized time interval of 0.2 showing the acoustic wave generation and interaction, underexpanded jet

tour lines while compressed regions are represented by continuous contour lines. Initially the nozzle lip is covered by a compression region which is followed by a rarefaction region in Fig.13a. Figs.13a-c show the development of an acoustic fluctuation (compressive in nature) as the boundary of a compressive part of the hydrodynamic fluctuation bulges out radially. The newly formed compressive region then breaks up into two halves. The upper half with a length scale corresponding to the acoustic wave moves upstream while the lower half forms a part of the hydrodynamic fluctuation of a smaller length scale and proceeds downstream. This is seen in Fig.13d. This interaction of the hydrodynamic fluctuations with the upstream moving acoustic wave resulting in the creation of acoustic fluctuations has been studied experimentally by Panda [11] where a similar creation of a rarefaction region is described but this phenomenon has not been reported in previous computational results. Fig.13e is similar to Fig.13a, the only difference is the change in polarity of the waves. Thus, Figs.13a-e represent a time period for the upstream moving acoustic waves in the jet screech mechanism.

Conclusions

A higher-order WENO scheme based numerical method is used to solve the axisymmetric Navier Stokes equations towards studying the supersonic jet screech phenomenon in imperfectly expanded circular jets. A validation exercise is initially carried out for supersonic circular jet flow by simulating a perfectly expanded jet. This numerical technique is then used to investigate both quantitative and qualitative aspects of the supersonic screech mechanism in imperfectly expanded circular jets. The present computations are used to predict sound pressure levels, screech amplitude, frequency and shock spacing in imperfectly expanded jets. These time-dependent computations also bring out essential aspects of a screeching jet phenomenon like the amplification and interaction of instability waves generated at the nozzle lip with the shock train in the stream-wise direction, generation and propagation of acoustic waves in the upstream direction which reflected from the nozzle lip destabilizes the shear layer and helps in amplification of instability waves completing the screech cycle. The generation of acoustic fluctuations due to the interaction of downstream moving hydrodynamic fluctuations with the upstream moving acoustic waves has been observed experimentally but has not been reported in previous computations.

Quantitative data obtained from numerical simulation of supersonic screech simulations sometimes do not match well with experimental data even when there is good qualitative agreement. This can be partly attributed to the fact that screech frequency and amplitude are influenced by sound reflecting surfaces present in the vicinity of the jet. Such surfaces are commonly present during experiments and can be in the form of a flange or nozzle body. Numerical simulations try to model the ideal case of an unbounded domain using non-reflecting boundary conditions. Axisymmetric computations as that presented here tend to display stronger subharmonics as compared to experimental results and three-dimensional computations. It has been suggested that this is a consequence of artificially confining the flow to be axisymmetric in such numerical formulations. Improved predictions are also expected by improving the turbulence modeling by incorporating a complete LES model instead of the simplified version used presently.

References

1. Powell, A., "On the Mechanism of Chocked Jet Noise", Proceedings of Phys. Soc. London, Vol.66, 1953, pp.1039-1056.

2. Powell, A., "On the Noise Emanating from a Two-Dimensional Jet above the Critical Pressure", Aeronautical Quarterly, Vol.4, 1953, pp.103-122.

3. Powell, A., "The Reduction of Choked Jet Noise", Proceedings of the Physical Society of London, Vol.B67, 1954, pp.313-327.

4. Raman, G., "Supersonic Jet Screech : Half-Century from Powell to the Present", Journal of Sound and Vibration, Vol.225, 1999, pp.543-571.

5. Harten, A. and Osher, S., "Uniformly High-Order Accurate Non-oscillatory Schemes I", SIAM Journal Numerical Analysis, Vol.24, No.2, 1987, pp.279-309.

6. Jiang, G.S. and Shu, C.W., "Efficient Implementation of Weighted ENO Schems", Journal of Computational Physics, Vol.126, 1996, pp.202-228.

7. Seiner, J., McLaughlin, D. and Liu, C., "Supersonic Jet Noise Generated by Large-Scale Instabilities", NASA, Technical Paper 2072, 1982.

8. Rona, A. and Zhang, X., "Time Accurate Numerical Study of Turbulent Supersonic Jets", Journal of Sound and Vibration, Vol.270, 2004, pp.297-321.

9. Jorgenson, P.C.E. and Loh, C.Y., "Computing Axisymmetric Jet Screech Tones Using Unstructured Grids", AIAA Paper 2002-3889, 2002.

10. Ponton, M., Seiner, J. and Brown, M., "Near Field Pressure Fluctuations in the Exit Plane of a Choked Axisymmetric Nozzle", NASA Technical Memorandum 113137, 1997.

11. Panda, J., "An Experimental Investigation of Screech Noise Generation", J. Fluid Mech., Vol.378, 1999, pp.71-96.

12. Panda, J., "Shock Oscillation in Under expanded Screeching Jets", J. Fluid Mech., Vol.363, 1998, pp.173-198.

13. Seiner, J., Manning, J. and Ponton, M., "The Preferred Mode of Instability for a Mach 2 Jet", AIAA Paper 86-1942, 1986.

14. Moin, P., Squires, K., Cabot, W. and Lee S., "A Dynamic Subgrid-Scale Model for Compressible Turbulence and Scalar Transport", Physics of Fluids A, Vol.3(11), 1991, pp.2746-2757.

15. Loh, C.Y. and Hultgren, L.S., "Jet Screech Noise Computation", NASA Technical Memorandum 212626, 2003.

16. Seiner, J. and Ponton, M., "Aeroacoustics Data for High Reynolds Number Supersonic Axisymmetric Jets", NASA Technical Memorandum 86296, 1985.

17. Norum, T. and Seiner, J., "Measurements of Mean Static Pressure and Far-field Acoustic of Shock-containing Supersonic Jets", NASA, Technical Memorandum 84521, 1983.

18. Seiner, J. and Norum, T., "Aerodynamic Aspects of Shock Containing Jet Plumes", AIAA Paper 80-0965, 1980.